Journal of Theoretical and Applied Vibration and Acoustics 6(1) 69-80 (2020)

I S A V

Journal of Theoretical and Applied

Vibration and Acoustics

journal homepage: http://tava.isav.ir

Numerical modeling of the propagation of ultrasonic waves in AISI 316L welds made by SMAW and GTAW processes

Seyyed Hossein Hosseini [a], **Farhang Honarvar** [b*]

[a] *Ph.D. Candidate, K. N. Toosi University of Technology, Tehran, Iran*

[b] *Professor, K. N. Toosi University of Technology, Tehran, Iran*

ARTICLE INFO

Article history:
Received 3 February 2020

Received in revised form
5 April 2020

Accepted 3 May 2020

Available online 14 May 2020

Keywords:
Ultrasonic technique,

Austenitic weld,

FE Simulation,

SMAW,

GTAW.

ABSTRACT

Ultrasonic evaluation of austenitic welds has long been considered to be difficult. Recent studies in this field have made it possible to inspect these welds in many cases. However, the ultrasonic inspection methods of austenitic steels are more complicated and limited than those of ferritic steels. The difficulty in ultrasonic testing of austenitic welds stems from the presence of anisotropic and expanded grains, which are usually in the form of columnar structures. These grain structures lead to local anisotropy in these types of welds. This paper aims to create a more thorough understanding of the propagation of ultrasonic waves in austenitic welds produced by gas tungsten arc welding and shielded metal arc welding processes. For this purpose, special finite element models are developed for these two types of welds. In these finite element models, the orientation of the structural domains in welds is accounted for in both SMAW and GTAW processes. Results are validated by comparison of the numerical models with theoretical predictions and experiments already reported in the literature. The numerical models provide a better understanding of how ultrasonic waves propagate in anisotropic structures of SMAW and GTAW welds.

1. Introduction

The applications of austenitic stainless steels in various industries are widespread [1]. Desirable properties of these materials such as suitable weldability, excellent corrosion and oxidation resistance [2], good creep resistance at elevated temperatures, and high toughness and strength

* Corresponding author:
E-mail address: honarvar@kntu.ac.ir (F. Honarvar)

http://dx.doi.org/10.22064/tava.2021.111405.1141

have resulted in various applications of austenitic stainless steels in different industries [3]. The austenitic stainless steel microstructure is remarkably different from the one in ferritic steel. This difference is due to the lack of phase transformation in the weld metal during the slow cooling process which causes dendritic structures with coarse grains. This complicated microstructure leads to anisotropic properties in these kinds of welds [4]. Austenitic welds should be inspected for safety and quality and this is usually done by non-destructive tests. Ultrasonic testing is widely used for inspecting various parts due to its ability to measure the size and depth of different kinds of defects [5, 6]. However, ultrasonic testing of austenitic welds has long been considered to be extremely difficult [7]. This is mostly due to high levels of attenuation and scattering in these welds. Some other phenomena like skewing and beam splitting, furthermore, gets in the way of the interpretation of test results [5]. The effect of these complexities on the interpretation of results has been investigated in several studies [7-9]. To optimize the UT process, one needs to have a comprehensive knowledge of the propagation of waves in austenitic steel weld metals [10]. The complexity of the governing equations in the propagation of ultrasonic waves in cases where the system geometry and the material specifications are complex has made the use of analytical equations very difficult and sometimes impossible. Moreover, in cases where there is a solution, the governing equations can only be solved by numerical methods [11]. To better understand the behavior of ultrasonic wave propagation and to examine the related parameters, various studies have been carried out. Ploix *et al*. investigated the ultrasonic scattering attenuation in austenitic stainless steel welds using numerical modeling [10]. Bond studied different ways to simulate the ultrasonic waves in solid media [11]. Ludwig *et al*. investigated the propagation and also scattering of ultrasonic waves in aluminum [12]. Yim *et al*. developed a mass-spring model in order to numerically simulate the propagation of elastic waves in solids [13].

In this study, we use finite element modelling (FEM) to study the propagation of ultrasonic waves in two austenitic weld samples; one prepared by gas tungsten arc welding (GTAW) and the other by shielded metal arc welding (SMAW). Our purpose is to verify if the difference in the behavior of ultrasonic waves in these two materials can be attributed to their grain structure. For this purpose, we measure the grain orientation on the two samples and try to reproduce them in our FEM models. The velocity and beam skewing in the FEM models and actual samples are then compared to see how closely the models represent the real samples.

2. Test Samples

The finite element models are developed based on real weld samples. Therefore, we first review these weld samples. The test samples used in this paper are the same as those reported by the authors in [14]. They are made of austenitic steel AISI 316L. This type of stainless steel is widely used in many industries.

The two weld specimens were produced by gas tungsten arc welding (GTAW) and shielded metal arc welding (SMAW) processes. Both samples were welded in a flat position. The dimensions of the weld samples are shown in Fig. 1.

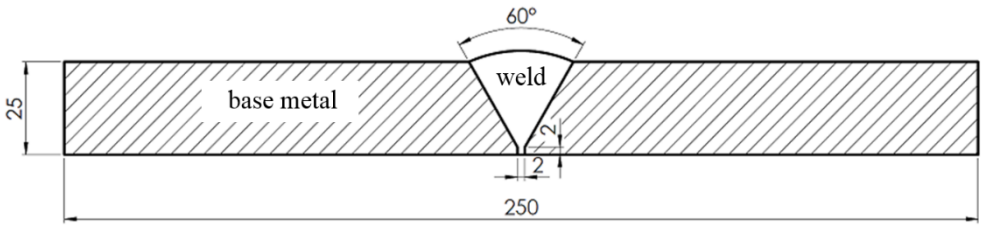

Fig. 1. Dimensions of the welds in millimeters.

Some weld samples were cut from the weld metal and the base metal so as to investigate the anisotropy in the base metal, SMAW metal, and GTAW metal. The samples had a cubic shape with a side length of 15 mm. The measurement of the wave velocities in the base metal and the welds were carried out in several directions along the main axes as well as non-principal axes with the angle of 45° with respect to the main axes.

A 2 MHz contact probe was used for measuring the longitudinal wave velocities. The dimensions of the samples that were cut from the welds to investigate the grain orientation in the welds were $5 \times 25 \times 40$ mm^3. The characteristics of the etching solution which was used to study the grain orientation in the weld metals are presented in Table 1.

Table 1. The characteristics of the etching solution used to study the grain orientation in welds.

Chemicals	Amounts
Ammonium persulphate	1.5 g
H_2O	7.5 ml
Iron perchloride	25 g
HCl	10 ml
HNO_3	3 ml

3. Characterization of austenitic welds

In the characterization of austenitic welds, the grain orientation and degree of anisotropy are two important factors that should be taken into consideration. The direction of grain growth and the columnar grain structure can be clearly seen in the metallographic pictures of the two welds samples. The grain orientations in the SMAW and GTAW welds are quite different as depicted in Figs. 2(a) and 3(a). Figs. 2(b) and 3(b) show the schematic of grain orientation in the SAMW and GTAW welds.

As shown in Figs. 2(a) and 3(a), the macrostructure images obtained from the austenitic welds clearly show the structure of the pillar grains and the initial growth perpendicular to the surface of the weld preparation. There is a significant difference between the direction of the grains and the extent of epitaxial growth in the two types of welds. In the case of the SMAW weld sample (Fig. 3), the penetration is not deep, and the grains are leaned to the left and right sides as they move away from the centerline. Furthermore, the extension of the columnar grains passes through several layers. A more complex structure is observed in the GTAW weld sample, which has a greater penetration depth compared to the SMAW weld. The grains in this type of weld are in the form of inverted "V" as shown in Fig. 2.

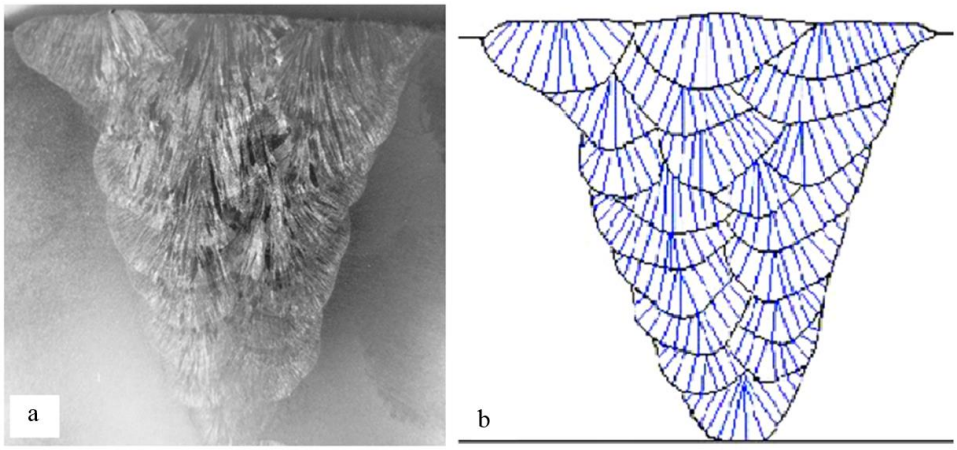

Fig. 2. (a). Macrostructure of the austenitic weld produced by GTAW process, (b) The austenitic weld grain orientation pattern produced by GTAW process.

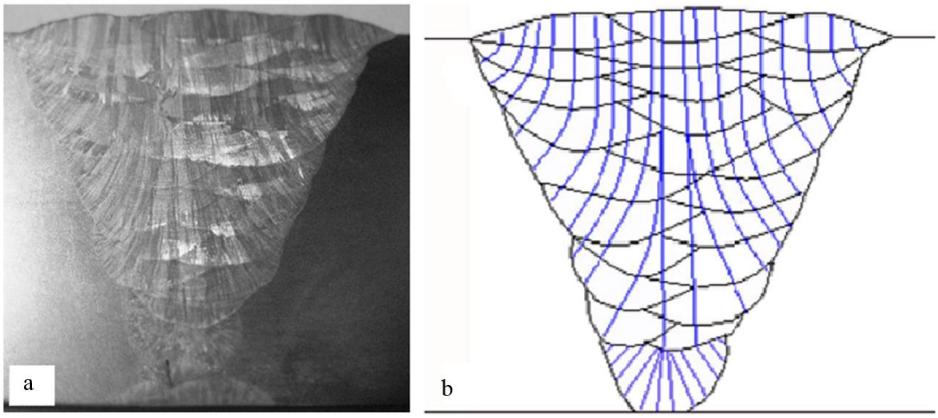

Fig. 3. (a). Macrostructure of the austenitic weld produced by SMAW process, (b) The austenitic weld grain orientation pattern produced by SMAW process.

In fact, the grains grow toward the center of each pass or direction of the temperature gradient. However, in the weld structure of the GTAW process, this epitaxial growth is not the same as the structure of the SMAW process, and the stretching of the grains through the weld layers does not exceed three weld passes. Epitaxial growth depends on the location of the welding passes. In the case that a weld pass lays directly on top of the lower pass, the epitaxial grain growth is more likely to happen. Generally, the solidification structure in multipass welds depends on several factors, such as the shape of the weld pool, the composition of the filler and the base metals, and the weld geometry. Considering that the other factors are constant, one of the most important factors in this structure is the shape of the weld pool. It depends on the type of welding process, and its parameters. Parameters such as thermal concentration, heat input, welding speed, temperature gradient direction, angle of inclination of the electrode, welding condition, position and arrangement of passes in the welding process play significant roles in shaping the pool. It should be noted that the type and rate of the gas flow in the GTAW process affect the shape of the weld pool too [15, 16].

The degree of anisotropy is a very important factor in ultrasonic evaluation. Anisotropy can affect the attenuation of the waves by beam skewing which depends on the material elastic constants matrix. Austenitic welds are often considered to be orthotropic. The matrix of elastic constants can be calculated through the measurement of the wave velocities in the media [17-19]. Christoffel equation is used to show the elastic properties of materials [20]:

$$\left|\lambda_{im} - \rho\upsilon^2\delta_{im}\right| = 0 \tag{1}$$

where λ_{im}, υ and ρ are Christoffel acoustic tensor, velocity, and the density, respectively. The Christoffel acoustic tensor is as follows [20]:

$$\lambda_{im} = C_{iklm}n_k n_l \tag{2}$$

where C_{iklm} is the material stiffness tensor and n_k and n_l are the normal direction cosines. One of the methods to calculate the material stiffness tensor is through the measurement of the ultrasound wave velocities in various directions. The material density is needed for calculating the matrix of the elastic constants as well. The densities of the SMAW weld sample, the GTAW sample, and the base metal are given in Table 3 [14].

Table 3. The densities of the SMAW weld sample, the GTAW weld sample, and the base metal.

Material	Density (kg/m^3)
Gas tungsten arc welding sample	7745
Shielded metal arc welding sample	8021
Base metal	7968

4. Finite Element Simulations

Simulation of ultrasonic wave propagation requires the modeling of the piezoelectric transducer. Two approaches can be taken. Either a piezoelectric element can be used or the effect of the piezoelectric transducer can be introduced into the model by application of a transient excitation pulse to the weld surface. The second approach is used here by applying the following excitation pulse to the model:

$$Y(t) = \begin{cases} \cos(2\pi ft)[1-\cos(\frac{2\pi f}{N}t)] & 0 \le t \le \frac{N}{f} \\ 0 & otherwise \end{cases} \tag{3}$$

where f is the frequency and N is the number of cycles [21]. The pulse shape for N = 3 and f = 2 MHz is shown in Fig. 4.

This pulse is exerted on the nodes that are at the interface of the weld surface and the transducer. The contact line between the transducer and the weld surface was simulated by using various point forces operating on the weld.

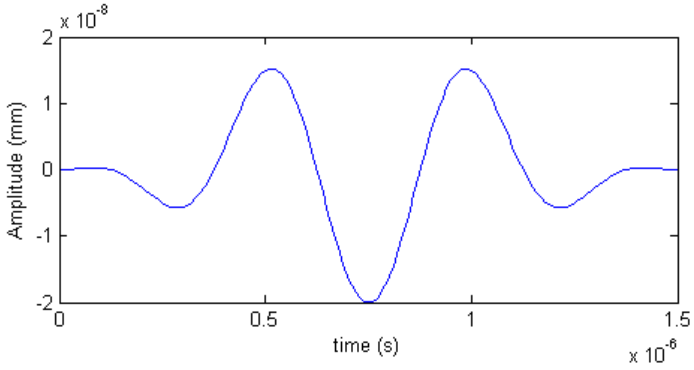

Fig. 4. Excitation pulse with a frequency of 2 MHz used in simulations.

The austenitic macroscopic structure and the orientation of the grains were defined in the software by dividing the weld cross section into various domains which were extracted from the weld cross sections as shown in Fig. 5. A typical ultrasonic wave propagating in the GTAW and SMAW weld FEM models are shown in Fig. 6.

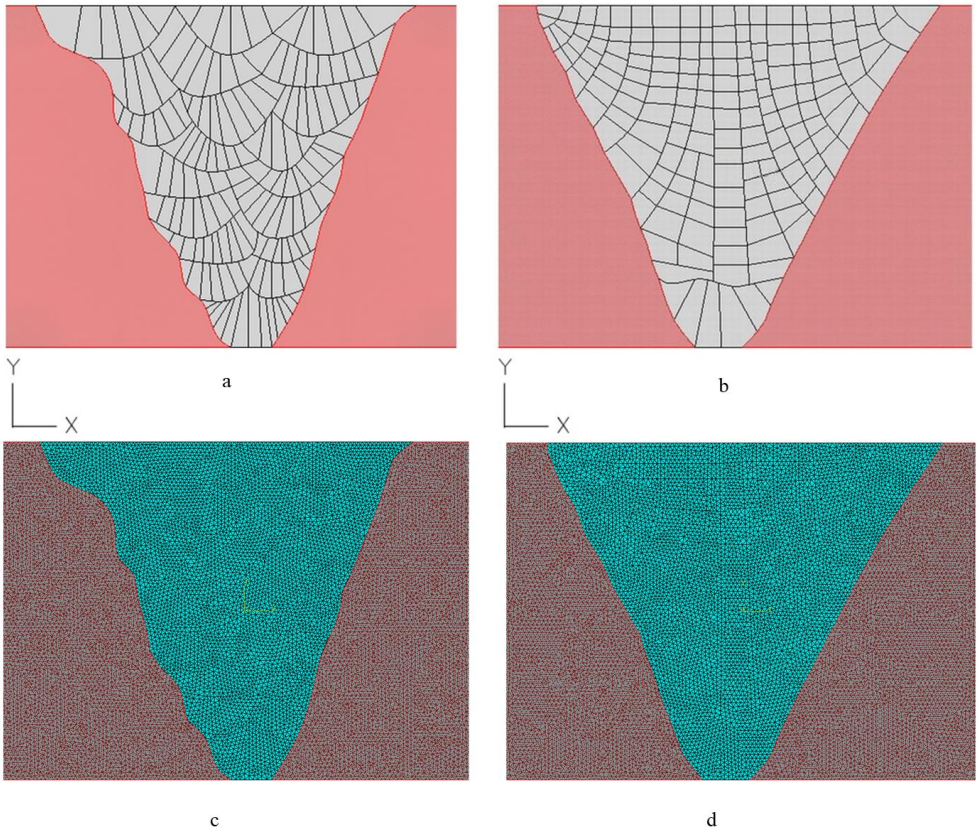

Fig. 5. The finite element model of the austenitic weld samples in which the welded section is divided into several structural domains for assigning the corresponding matrix of elastic constants: (a) the weld cross section obtained from the GTAW process, (b) the weld cross section obtained from the SMAW process, (c) the mesh used for the GTAW model, (d) the mesh used for the SMAW model.

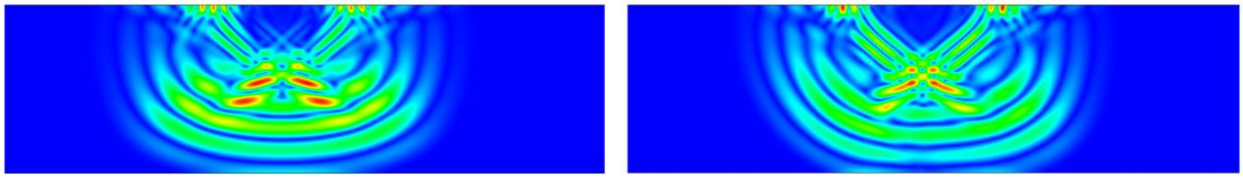

a b

Fig. 6. The finite element model of the propagation of ultrasonic waves in austenitic weld samples: (a) GTAW model, (b) SMAW model.

The matrix of elastic constants, *C*, of a material can be formed through the measurement of the elastic constants using ultrasonic waves and incorporating the Christoffel equation. The method of determining *C* is commonly referred to as the cube-cutting technique [20]. To make the required measurements, cubes were cut from the original specimen at various orientations to the main axes, and wave velocity measurements were carried out on them [20]. The matrices of the elastic constants of the shielded metal arc welding sample, the gas tungsten arc welding sample, and the base metal, were reported in [14] as:

$$C_{BM} = \begin{bmatrix} 265.5 & 121.8 & 110.2 & 0 & 0 & 0 \\ 121.8 & 265.5 & 112.9 & 0 & 0 & 0 \\ 110.2 & 112.9 & 265.5 & 0 & 0 & 0 \\ 0 & 0 & 0 & 79.2 & 0 & 0 \\ 0 & 0 & 0 & 0 & 76.5 & 0 \\ 0 & 0 & 0 & 0 & 0 & 77.9 \end{bmatrix} \text{GPa} \tag{4}$$

$$C_{SMAW} = \begin{bmatrix} 258.5 & 178.7 & 131.8 & 0 & 0 & 0 \\ 181.7 & 225.1 & 164.2 & 0 & 0 & 0 \\ 131.8 & 163.9 & 208.9 & 0 & 0 & 0 \\ 0 & 0 & 0 & 115.3 & 0 & 0 \\ 0 & 0 & 0 & 0 & 101.1 & 0 \\ 0 & 0 & 0 & 0 & 0 & 74.2 \end{bmatrix} \text{GPa} \tag{5}$$

$$C_{GTAW} = \begin{bmatrix} 278.6 & 173.7 & 148.1 & 0 & 0 & 0 \\ 173.7 & 254.9 & 112.1 & 0 & 0 & 0 \\ 148.1 & 112.1 & 247.2 & 0 & 0 & 0 \\ 0 & 0 & 0 & 106.5 & 0 & 0 \\ 0 & 0 & 0 & 0 & 73.9 & 0 \\ 0 & 0 & 0 & 0 & 0 & 74.3 \end{bmatrix} \text{GPa} \tag{6}$$

the anisotropic factor is determined as [22]:

$$A = \frac{2C_{44}}{C_{11} - C_{12}} \tag{7}$$

To introduce the anisotropic structure of the welds into the finite element model, the matrix of elastic constants obtained from the experiments (Eqs. 4 to 6) is rotated according to the grain orientation relative to the y axis in each of the SMAW and GTAW welding samples. Then, the matrix of each of the structural domains (shown in Fig. 5) is assigned to the corresponding domain under a certain angle. For the elastic constant matrices acquired, the anisotropic factors were calculated to be 1.1 for the base metal, 2.9 for the SMAW weld, and 2.0 for the GTAW weld. In isotropic materials, *A* is equal to 1. Therefore, with an anisotropic factor of 1.1, the base

metal is almost isotropic. Besides, the matrix of the elastic constants of the base metal shows that the base metal crystal structure can be assumed to be cubic. The austenitic stiffness matrix also confirms the orthotropic structure for the welds generated by the SMAW and GTAW processes.

5. Discussion

In anisotropic materials, like austenitic steels, The beam skewing phenomena occurs because of the difference between the group velocity and phase velocity [4]. Therefore, the wavefront will not be perpendicular to the beam axis as shown in Fig. 7.

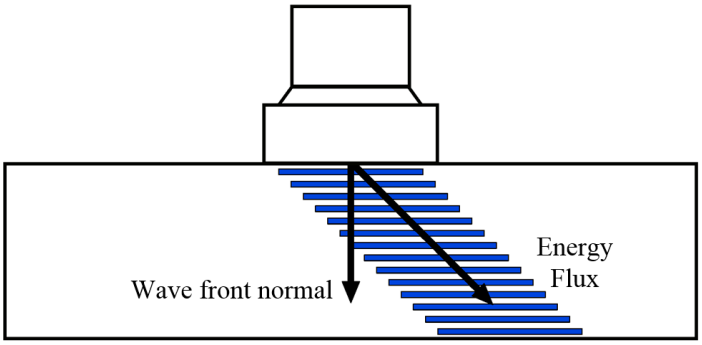

Fig. 7. Beam skewing in austenitic welds.

To measure the velocities of ultrasonic waves in the base metal, SMAW, and GTAW welds, several samples of each material were cut at different angles and the velocity of the longitudinal wave was measured in each of them. Longitudinal wave velocities were also measured in the corresponding finite element models. The measured velocity of each material as a function of the beam direction is shown in Fig. 8.

As a result, the beam skewing is a function of the angle between the material grain orientation and the direction of the ultrasonic beam. Figures 8(a), (c), and (e) show the phase velocity and Figs. 8(b), (d), and (f) show the beam skewing in the base metal, SMAW weld sample, and GTAW weld sample on the *XY* plane, respectively as depicted in Fig. 5. The beam skewing is determined from the angle between the group velocity and phase velocity. Figure 8(c) demonstrates that the longitudinal phase velocity for the shielded metal arc welding sample changes from 5190 to 6280 m/s with respect to the propagation angle. These variations in the finite element simulation are from 5160 to 6135 m/s. This variation range for the gas tungsten arc welding sample, shown in Fig. 8(e), changes from 5550 to 6060 m/s in experiments and from 5850 to 5890 m/s in simulations. By comparison of the velocities of the longitudinal waves in the SMAW and GTAW weld metals, it can be concluded that due to the difference in the maximum and minimum wave velocities in the SMAW weld metal, the anisotropy in this weld is higher than that of the GTAW weld sample. The comparison of the anisotropic factor obtained from the matrices of elastic constants for the two welds also confirms this conclusion (Eqs. 4 to 7). Pearson correlation coefficient [23] of the phase velocity curves in SMAW weld obtained from simulation and experiments is 0.983.

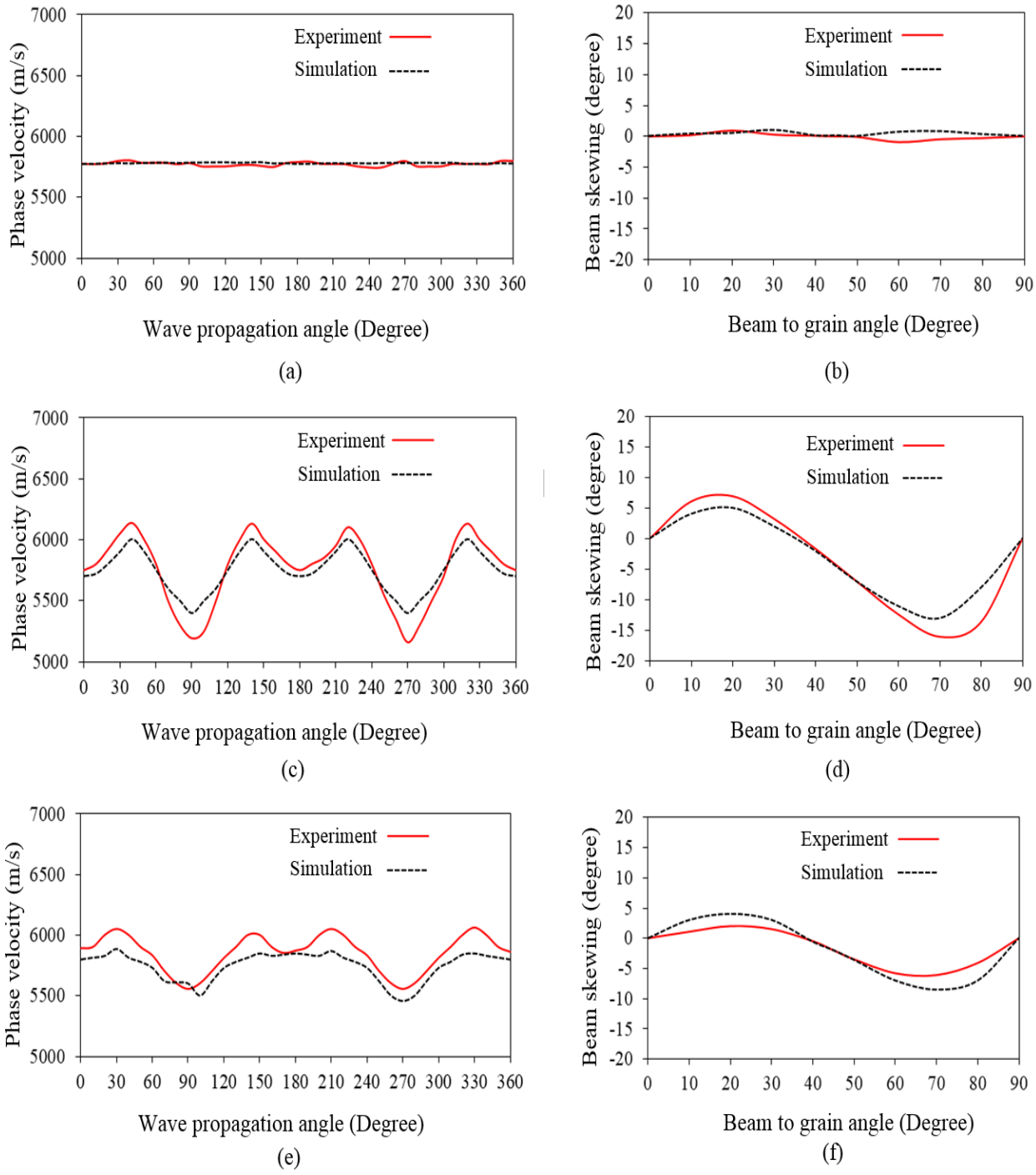

Fig. 8. (a) Phase velocity in the base metal, (b) beam skewing in the base metal, (c) phase velocity in the shielded metal arc welding sample, (d) beam skewing in the shielded metal arc welding sample, (e) phase velocity in the gas tungsten arc welding sample, and (f) beam skewing in the gas tungsten arc welding sample.

This value is 0.938 for GTAW weld metal and 0.918 for the base metal. These coefficients show that the FEM models represent the real samples very well. Figure 8(d) demonstrates that the maximum angle between the vector of the phase velocity and the vector of the group velocity (beam skewing) for longitudinal waves in the SMAW weld is 16.5° in the experiments and 13.1° in simulations. These values are 6.3° and 8.8° for the GTAW weld, respectively, see Fig. 8(f). By comparing the beam skewing curves of the two types of the welds, it can be observed that beam skewing in the shielded metal arc welding sample is higher than that of the gas tungsten arc welding sample.

Pearson correlation coefficient of the beam skewing curves in SMAW weld obtained from simulations and experiments is 0.984. This value is 0.983 for GTAW weld sample and 0.894 for the base metal. It can be concluded that the experimental results are in good agreement with the results obtained from simulations. In addition, the relatively low anisotropic factor in the AISI316L base metal and the approximately linear shape of its velocity and beam skewing curves indicate that this material almost isotropic, Figs. 8(a) and 8(b).

6. Conclusion

In this paper, the propagation of ultrasonic waves in austenitic steel welds prepared by two different welding processes was studied. The two welding processes considered are shielded metal arc welding (SMAW) and gas tungsten arc welding (GTAW). The anisotropic and heterogeneous structure along with large elongated grains of austenitic welds makes the ultrasonic testing of these welds very difficult. A novel finite element model was developed to simulate the weld structure in which the material orientation of the structural subdomains was taken into consideration. Finite element simulations of ultrasonic wave propagation in these welds showed that the anisotropy in SMAW sample is greater than that of the GTAW sample. Comparison of finite element results with experimental measurements confirmed the validity of the developed model. By comparing the longitudinal phase velocities in SMAW and GTAW welds, it was found that the difference between the minimum and maximum wave velocities in SMAW sample is larger than that of the GTAW sample. For the base metal, this difference was found to be insignificant. The beam skewing in the SMAW sample was also found to be larger than that of the GTAW sample. It is concluded that different welding processes and different operating parameters can result in completely different weld structures. The proposed FE model can be used for predicting the behavior of ultrasonic waves in these welds and help in developing more efficient test procedures.

References

[1] X. Edelmann, Ultrasonic examination of austenitic welds at reactor pressure vessels, Nuclear engineering and design, 129 (1991) 341-355.
[2] A. Harker, J. Ogilvy, J. Temple, Modeling ultrasonic inspection of austenitic welds, Journal of Nondestructive Evaluation, 9 (1990) 155-165.

[3] J. Ford, R. Hudgell, A final report on the performance achieved by non-destructive testing of defective butt welds in 50mm thick Type 316 stainless steel, in, UKAEA Risley Nuclear Power Development Establishment, 1987.
[4] D.S. Kupperman, K.J. Reimann, Ultrasonic wave propagation and anisotropy in austenitic stainless steel weld metal, in, Argonne National Lab., IL, 1980.
[5] J. Tomlinson, A. Wagg, M. Whittle, Ultrasonic inspection of austenitic welds, (1980).
[6] J. Moysan, A. Apfel, G. Corneloup, B. Chassignole, Modelling the grain orientation of austenitic stainless steel multipass welds to improve ultrasonic assessment of structural integrity, International Journal of Pressure Vessels and Piping, 80 (2003) 77-85.
[7] P. Kemnitz, U. Richter, H. Klüber, Measurements of the acoustic field on austenitic welds: a way to higher reliability in ultrasonic tests, Nuclear engineering and design, 174 (1997) 259-272.
[8] S. Halkjær, M.P. Sørensen, W.D. Kristensen, The propagation of ultrasound in an austenitic weld, Ultrasonics, 38 (2000) 256-261.
[9] B. Chassignole, D. Villard, G.N. Van Chi, N. Gengembre, A. Lhémery, Ultrasonic propagation in austenitic stainless steel welds - approximate model and numerical methods results and comparison with experiments, in: Review of progress in quantitative nondestructive evaluation: Volume 19, AIP Publishing, 2000, pp. 153-160.
[10] M.-A. Ploix, P. Guy, B. Chassignole, J. Moysan, G. Corneloup, R.E. Guerjouma, Measurement of ultrasonic scattering attenuation in austenitic stainless steel welds: Realistic input data for NDT numerical modeling, Ultrasonics, 54 (2014) 1729-1736.
[11] L. Bond, Methods for the computer modelling of ultrasonic waves in solids, Research techniques in nondestructive testing., 6 (1982) 107-150.
[12] R. Ludwig, W. Lord, A finite-element study of ultrasonic wave propagation and scattering in an aluminum block, Materials evaluation, 46 (1988) 108-113.
[13] H. Yim, Y. Sohn, Numerical simulation and visualization of elastic waves using mass-spring lattice model, IEEE transactions on ultrasonics, ferroelectrics, and frequency control, 47 (2000) 549-558.
[14] S.M. Tabatabaeipour, F. Honarvar, A comparative evaluation of ultrasonic testing of AISI 316L welds made by shielded metal arc welding and gas tungsten arc welding processes, Journal of Materials Processing Technology, 210 (2010) 1043-1050.
[15] S. Lu, H. Fujii, K. Nogi, Arc ignitability, bead protection and weld shape variations for He–Ar–O 2 shielded GTA welding on SUS304 stainless steel, Journal of materials processing technology, 209 (2009) 1231-1239.
[16] M. Jou, Experimental study and modeling of GTA welding process, Journal of manufacturing science and engineering, 125 (2003) 801-808.
[17] A. Mouchtachi, R. El Guerjouma, J. Baboux, P. Santini, P. Merle, D. Bouami, Ultrasonic study of elastic anisotropy of material composite, Applied Composite Materials, 11 (2004) 341-351.
[18] T.-T. Wu, Z.-H. Ho, Anisotropic wave propagation and its applications to NDE of composite materials, Experimental Mechanics, 30 (1990) 313-318.
[19] B. Dewey, L. Adler, R. King, K. Cook, Measurements of anisotropic elastic constants of type 308 stainless-steel electroslag welds, Experimental Mechanics, 17 (1977) 420-426.
[20] J.L. Rose, Ultrasonic waves in solid media, Cambridge university press, 2004.
[21] G. Baskaran, C.L. Rao, K. Balasubramaniam, Simulation of the TOFD technique using the finite element method, Non-Destructive Testing and Condition Monitoring, 49 (2007) 641-646.

[22] C. Zener Elasticity and Anelasticity of Metals, University of Chicago Press, Chicago, Illinois 1948.
[23] J.L. Rodgers, W.A. Nicewander, Thirteen Ways to Look at the Correlation Coefficient, The American Statistician, 42 (1988) 59-66.